

Patterns and trends in Chlorophyll-a concentration and phytoplankton phenology in the biogeographical regions of Southwestern Atlantic

Ana Laura Delgado¹, Ismael Hernández-Carrasco², Vincent Combes³, Joan Font-Muñoz⁴, paula pratolongo⁵, and Gotzon Basterretxea⁶

¹Instituto Argentino de Oceanografía (IADO-CONICET))

²Mediterranean Institute for Advanced Studies

³Oregon State University

⁴Institut Mediterrani d'Estudis Avancats (IMEDEA-UIB-CSIC)

⁵CERZOS-CONICET-UNS

⁶IMEDEA (CSIC-UIB)

April 3, 2023

Abstract

The Southwestern Atlantic Ocean (SAO), is considered as one of the most productive areas of the world, with high abundance of ecologically and economical important fish species. Yet, the biological responses of this complex region to climate variability are still uncertain. Here, using 24 years of satellite derived Chl-a datasets, we classified the SAO into coherent regions based on homogeneous temporal variability of Chl-a concentration, as revealed by the SOM (Self-Organizing Maps) analysis. These coherent biogeographical regions were the basis of our regional trend analysis in phytoplankton biomass, regional phenological indices, and environmental forcing variations. A generalized positive trend in phytoplankton concentration is observed, especially in the highly productive areas of the northern shelf-break, where phytoplankton biomass is increasing at an outstanding rate up to 0.42 ± 0.04 mg m⁻³ per decade associated with the sea surface temperature (SST) warming (0.11 ± 0.02 °C decade⁻¹) and the mixed layer depth shoaling (-3.36 ± 0.13 m decade⁻¹). In addition to the generalized increase in chlorophyll, the most sticking changes in phytoplankton dynamics observed in the SAO are related to the secondary bloom that occurs in most of the regions (15 ± 3 and 24 ± 6 days decade⁻¹) which might be explained by the significant warming trend of SST, which would sustain the water stratification for a longer period, thus delaying the secondary bloom initialization. Consistent with previous studies, our results provided further evidences of the impact of climate change in these highly productive waters.

Hosted file

959361_0_art_1_rs0yc4.docx available at <https://authorea.com/users/541876/articles/632143-patterns-and-trends-in-chlorophyll-a-concentration-and-phytoplankton-phenology-in-the-biogeographical-regions-of-southwestern-atlantic>

Hosted file

959361_0_supp_10828396_rrzndw.docx available at <https://authorea.com/users/541876/articles/632143-patterns-and-trends-in-chlorophyll-a-concentration-and-phytoplankton-phenology-in-the-biogeographical-regions-of-southwestern-atlantic>

1 **Patterns and trends in Chlorophyll-a concentration and phytoplankton phenology in**
2 **the biogeographical regions of Southwestern Atlantic**

3 **Ana L. Delgado^{1,2}, Ismael Hernández-Carrasco³, Vincent Combes^{3,4}, Joan Font-Muñoz³,**
4 **Paula D. Pratolongo^{5,6} and Gotzon Basterretxea³**

5 ¹ Instituto Argentino de Oceanografía (IADO-CONICET-UNS), Bahía Blanca, 8000, Argentina.

6 ² Departamento de Geografía y Turismo, Universidad Nacional del Sur (UNS), Bahía Blanca,
7 8000, Argentina.

8 ³ Institut Mediterrani d'Estudis Avançats (IMEDEA-CSIC-UIB), Esporles, 07190, Spain.

9 ⁴ Departament de Física, Universitat de les Illes Balears, Palma de Mallorca, 07071, Illes
10 Balears, Spain.

11 ⁵ Centro de Recursos Renovables de la Región Semiárida (CERZOS-CONICET-UNS), Bahía
12 Blanca, 8000, Argentina.

13 ⁶ Departamento de Biología, Bioquímica y Farmacia, Universidad Nacional del Sur (UNS),
14 Bahía Blanca, 8000, Argentina.

15
16 Corresponding author: Ana L. Delgado (aldelgado@iado-conicet.gob.ar)

17 **Key Points:**

- 18 • Chlorophyll-a concentration has increased in the las 24-years in most of the Southwestern
19 Atlantic.
- 20 • Phytoplankton phenological changes have been observed, mainly on the autumn bloom.
- 21 • Phytoplankton abundance and phenology might be affected by the sea surface
22 temperature increase and the the mixed layer depth shoaling.
23

24 **Abstract**

25 The Southwestern Atlantic Ocean (SAO), is considered as one of the most productive areas of
26 the world, with high abundance of ecologically and economical important fish species. Yet, the
27 biological responses of this complex region to climate variability are still uncertain. Here, using
28 24 years of satellite derived Chl-a datasets, we classified the SAO into coherent regions based on
29 homogeneous temporal variability of Chl-a concentration, as revealed by the SOM (Self-
30 Organizing Maps) analysis. These coherent biogeographical regions were the basis of our
31 regional trend analysis in phytoplankton biomass, regional phenological indices, and
32 environmental forcing variations. A generalized positive trend in phytoplankton concentration is
33 observed, especially in the highly productive areas of the northern shelf-break, where
34 phytoplankton biomass is increasing at an outstanding rate up to $0.42 \pm 0.04 \text{ mg m}^{-3}$ per decade
35 associated with the sea surface temperature (SST) warming ($0.11 \pm 0.02 \text{ }^\circ\text{C decade}^{-1}$) and the
36 mixed layer depth shoaling ($-3.36 \pm 0.13 \text{ m decade}^{-1}$). In addition to the generalized increase in
37 chlorophyll, the most striking changes in phytoplankton dynamics observed in the SAO are
38 related to the secondary bloom that occurs in most of the regions (15 ± 3 and $24 \pm 6 \text{ days decade}^{-1}$)
39 which might be explained by the significant warming trend of SST, which would sustain the
40 water stratification for a longer period, thus delaying the secondary bloom initialization.
41 Consistent with previous studies, our results provided further evidences of the impact of climate
42 change in these highly productive waters.

43 **Plain Language Summary**

44 The Southwestern Atlantic Ocean (SAO), is one of the most biologically productive areas of the
45 world, with high abundance of fish species. This important area might be affected by the
46 environmental consequences of climate change. In this study we addressed the influence of the
47 already observed changes in environmental conditions on the phytoplankton, which is the base of
48 the marine food web, in the last 24 years. There is an increase in phytoplankton abundance as
49 well as the timing and intensity of the autumn bloom in some specific areas of the SAO. We
50 have found that these changes might be related to the increase of sea surface temperature and the
51 shoaling of the mixed layer depth, which is the upper layer of the ocean, which is directly
52 influenced by the atmospheric processes. Consistent with previous studies, our results provided
53 further evidences of the impact of climate change in these highly productive waters.

54 **1 Introduction**

55 Phytoplankton is at the base of the marine food webs and plays a major role on the global
56 CO_2 fluxes. Indeed, marine phytoplankton roughly produces 50 Gt of organic C yr^{-1} ,
57 corresponding to $\sim 40 \%$ of the annual global primary productivity contributing to the uptake of
58 more than 23% of the total anthropogenic CO_2 emissions into the atmosphere (Friedlingstein et
59 al., 2019). Phytoplankton community species composition, initiation, duration and therefore
60 intensity of blooms and the overall productivity of the oceans are predicted to change in response
61 to variations in water temperature, nutrients supply, and acidification derived from the ongoing
62 climate change (Doney et al., 2012). Phytoplankton growth is mostly controlled by light and
63 nutrient availability and therefore, tightly linked to the dynamics of the ocean surface mixed
64 layer (Longhurst, 2007). Atmospheric forcing and large-scale climate variability pattern, together
65 with top-down controls (i.e. grazing), modulate phytoplankton phenological cycles (Zhai et al.,
66 2013). Thus, the long-term variations in phytoplankton phenology may be used as indicators to

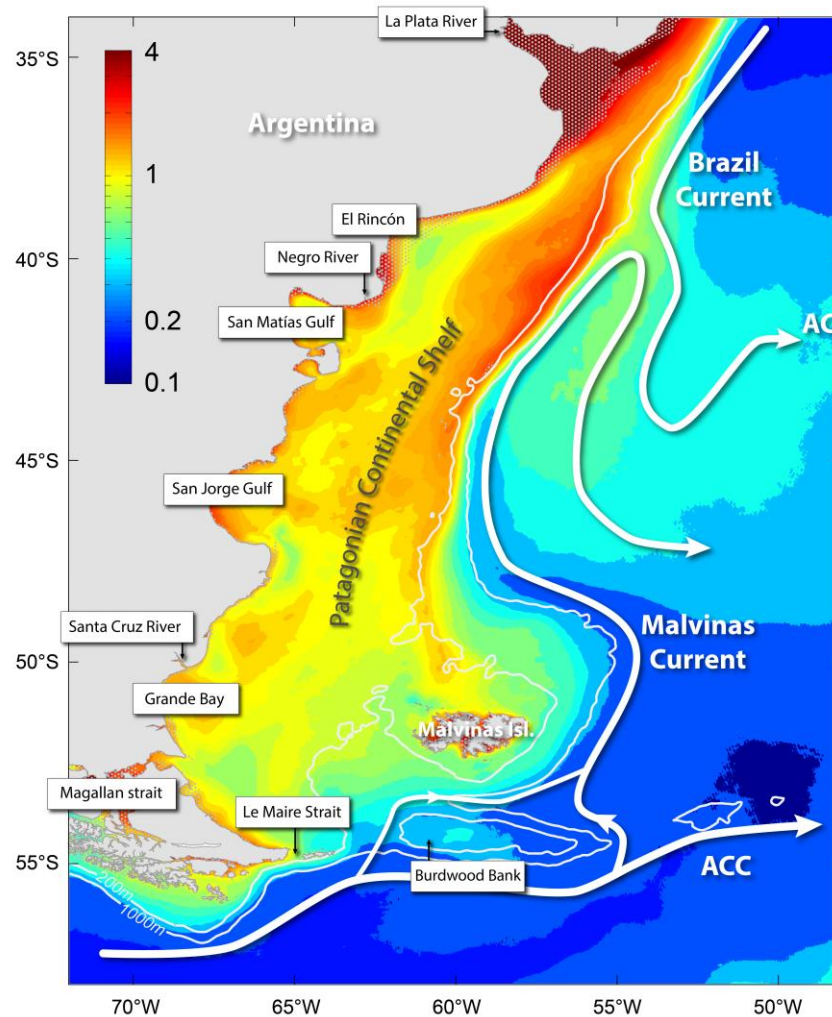
67 assess how variations in the marine environment propagate from primary producers to higher
68 trophic levels. However, anticipating how these changes will occur in a future ocean remains
69 challenging, as phytoplankton includes phylogenetically diverse organisms with disparate
70 metabolic responses and evolutionary backgrounds (Dutkiewicz, et al., 2013; Anderson et al.,
71 2021).

72 The Southwestern Atlantic Ocean is a vast sink for atmospheric and anthropogenic CO²
73 via biological and solubility pump processes (Sigman et al., 2010), and is regarded as one of the
74 most important regions for the global carbon cycle. This is largely due to the high biological
75 productivity that results from its intense hydrodynamics and biogeochemical features (Field et
76 al., 1998). The Patagonian shelf, which extends from the tip of South America (~55°S) to the
77 Brazil/Malvinas Confluence (~38°S), occupies less than 2 % of the Southern Ocean surface. Yet
78 it is one of the most biologically productive regions and largest carbon sink in the world, and one
79 of its potentially most important sources for iron fertilization to the rest of the Southern Ocean
80 (Fig.1, García et al., 2008; Lutz et al., 2010). This region is characterized by the presence of
81 intense frontal systems driven by the combination of different physical processes (i.e. coastal
82 upwelling, thermo-haline circulation, tidal forcing; Acha et al., 2004) which can lead to strong
83 phytoplankton blooms, mainly dominated by diatoms, coccolithophores and dinoflagellates (e.g.
84 Alvain et al., 2008; Guinder et al., 2018; Segura et al., 2021; Delgado et al., 2019). As a result of
85 climate change, the region is showing clear evidence of environmental changes, largely
86 associated with an increase in sea surface temperature (SST; Hobday and Pecl, 2014), changes in
87 wind patterns (Leyba et al., 2019), the poleward migration of western boundary currents (Artana
88 et al., 2019) and intensification and/or increase in the frequency and intensity of climate
89 variability events (ENSO, Southern Annular Mode, droughts, heatwaves; e.g. Cai et al., 2020;
90 Risaro et al., 2022).

91 The classification of marine areas into biogeographical regions sharing a similar dynamic
92 has become essential to understand the responses of marine ecosystems in highly complex areas,
93 such as the SAO, to environmental forces in present and future climate scenarios (Basterretxea et
94 al., 2018). In addition, classification of the marine environment into biogeographic regions
95 contributes to the understanding of ecosystem functions, very useful to define local (or specific)
96 indicators of ecosystem state, supporting the establishment of resource management and
97 conservation policies (Spalding et al., 2007). Satellite ocean-color data provides synoptic and
98 long-term coverage, which is ideal for regionalization studies. The Self-Organizing Maps
99 (SOMs), a neural network-based technique developed in the last decades, has proven very
100 effective to cluster and identify patterns in large datasets (Kohonen, 1982; Vesanto and
101 Alhoniemi, 2000). SOM classification method has been used for a variety of applications
102 including the synthesis of spatial patterns of chlorophyll-a (Chl-a) and its variation and the
103 classification of spectral signals for subsequent inference of phytoplankton groups (e.g. Saraceno
104 et al., 2006; Ben Mustapha et al., 2014; Basterretxea et al., 2018; Yala et al., 2020). SOM can be
105 applied to both space and time domains of the analysed variable, providing, a powerful analysis
106 tool for diagnosing ocean processes (Liu et al., 2016, Hernández-Carrasco and Orfila, 2018).

107 The present work aims at characterizing the spatial patterns and long-term trends of Chl-a
108 concentration and phytoplankton phenology in the Southwestern Atlantic Ocean, and their
109 relation with on-going climate-induced environmental changes in the Southwestern Atlantic.
110 Using 24 years of satellite derived Chl-a datasets, we first classified the SAO into coherent
111 regions based on homogeneous temporal variability of Chl-a concentration, as revealed by the

112 SOM analysis. These coherent biogeographical regions were the basis of our regional trend
 113 analysis in phytoplankton biomass, regional phenological indices, and environmental forcing
 114 variations. The observed changes in phytoplankton biomass and phenology, as well as the related
 115 environmental changes, are key to understand regional functional and structural aspects of
 116 marine communities in the SAO, allowing to set a potential strategy to detect and monitor crucial
 117 regions.



118

119 **Figure 1.** Mean Chlorophyll-a concentration (mg m^{-3}) in the Southwestern Atlantic Ocean
 120 (SAO) for the period (1998-2021) and, overlapped, main circulation patterns (thick arrows).
 121 Dotted areas indicate biased chlorophyll-a values that were excluded from the analysis.

122 2 Materials and Methods

123 2.1 Data sources

124 Our analysis is based on the sea surface Chl-a (mg m^{-3}) merged product provided by the
 125 GlobColour project (distributed by ACRI ST, France: <https://hermes.acri.fr/>). A spatial subset of
 126 the study area (Fig.1) was extracted from a time series of the 8-day L3 Chl-a product at 4 km

127 resolution for the period 1998-2021 (24 years). This ocean color product is the result of merging
128 SeaWiFS, MERIS, MODIS-Aqua and OLCI sensors and estimates the average Chl-a
129 concentration over the first optical depth (Maritorena et al., 2010). Merging data from different
130 satellite sensors is an effective method for increasing the study period of ocean color satellites to
131 access climatic studies (Maritorena and Siegel, 2005). The Chl-a algorithms used to develop this
132 product were validated in the Southwestern Atlantic Ocean with in situ data acquired between
133 2001 and 2019 obtaining accurate results (Delgado et al., 2021, $R^2=0.84$; Dogliotti et al., 2009,
134 $R^2=0.89$; Ferreira et al., 2013, $R^2=0.75$). Moreover, the GlobColour merged product presents a
135 good accuracy with in-situ Chl-a data ($R^2=0.81$, Bias=0.03; Garnesson et al., 2022). Even though
136 this product has not been climatology bias corrected, as OC CCI (Sathyendranath et al., 2019),
137 both products present similar accuracy results (Yu et al., 2023), plus GlobColour flag strategy
138 allows a higher spatial and temporal covering (Garnesson et al., 2019). Since global algorithms
139 (based on blue-to-green ratios) do not perform well in the optically complex waters of the inner
140 Argentinean Continental Shelf (Armstrong et al., 2004; Delgado et al., 2021; Williams et al.,
141 2013), we masked the coastal waters located at depths < 25 m to avoid biased results.

142 Physical variables used for the environmental characterization were obtained from the Global
143 Ocean Physics Reanalysis provided by CMEMS (GLORYS12v1). GLORYS provide monthly
144 Sea Surface Temperature (SST), monthly Mixed Layer Depth (MLD) and Sea Surface Salinity
145 (SSS), among other physical variables, at $1/12^\circ$ spatial resolution. GLORYS12 is available in
146 Copernicus Marine Environment Monitoring Service (CMEMS,
147 <https://data.marine.copernicus.eu>) and is based on the current real-time global high-resolution
148 forecasting CMEMS system PSY4V3 (Lellouche et al., 2018). The model outputs have proved to
149 present accurate results for trend analysis (SST, bias $< 0.01^\circ\text{C}$; SSS, bias < 0.2 ; Drévillon et al.,
150 2022).

151 2.2 Biogeographical regionalization

152 Biogeographical regions within the study area were defined based on the analysis of satellite
153 derived Chl-a using Self-Organizing Maps (SOM). SOM is a type of artificial neural network
154 that is trained using an unsupervised learning algorithm. This technique is especially suited for
155 feature extraction and pattern recognition in large datasets (Kohonen et al., 1982; 1990). SOM is
156 a nonlinear mapping method that projects high-dimensional data onto a low dimensional space,
157 preserving the topology of the original dataset. As a result, SOM can summarize the information
158 contained in large time series of georeferenced variables, into a single map of a few patterns (Liu
159 et al., 2016). When SOM is applied to the time domain of Chl-a satellite data, distinctive
160 temporal patterns of Chl-a concentration can be inferred, allowing the identification of regions
161 having a similar phytoplankton dynamics (Basterretxea et al., 2018).

162 We selected a network or map, of 3×3 neurons or units. Increasing the number of neurons, for
163 instance using a neural network of size of 4×4 and 4×3 , we obtain more detailed temporal
164 patterns, and more regions of Chl-a variability emerge. However, these new patterns only split
165 the boundaries of regions inferred from the 3×3 SOM, without providing relevant insight into
166 regions with different biochemical or physical behaviour. Furthermore, as reported in Liu et al.
167 (2006) and also seen in Basterretxea et al. (2018) and Hernández-Carrasco and Orfila (2018),

168 using larger number of neurons can result in fictitious patterns (with zero probability of
169 occurrence), which are not representative of the analysed data set.

170 In our computations we use a sheet and hexagonal map lattice configuration, guaranteeing that
171 the distance between the neuron and all its associated neighbours is the same. Each neuron has
172 assigned a weighted vector of Chl-a values randomly generated during the initialization. In the
173 training process the neural network is transformed through an iterative presentation of the
174 satellite Chl-a data, previously normalized. In each iteration (or epoch), the neuron whose weight
175 vector is more similar (in terms of Euclidean distance) to the input data vector, called Best-
176 Matching Unit (BMU), is updated together with its topological neighbours towards the input
177 sample following a neighbourhood function. Following Liu et al. (2006), we opted for a 'Ep'
178 type neighbourhood function and a batch training algorithm, as this combination yields the best
179 accurate patterns (i.e. lower quantitative and topological errors) and low computational cost.
180 After repeating the training process iteratively (100 epochs in our case), until a stable
181 convergence of the map is achieved, we obtain a neural network with the final time variability
182 patterns of Chl-a concentration. The resulting patterns will exhibit some similarity because the
183 SOM process assumes that a single sample of data (one input vector) contributes to the creation
184 of more than one pattern, as the whole neighbourhood around the best matching pattern is also
185 updated in each step of training. We have used the SOM v.2.0 MATLAB toolbox (Vesanto et al.,
186 2000) distributed by the Helsinki University of Technology (<http://www.cis.hut.fi/somtoolbox/>)
187 and adapted to long time series of satellite data.

188 2.3 Phytoplankton phenology

189 Phytoplankton phenology was analysed using the characteristic Chl-a time series obtained for
190 each biogeographical region from the SOM analysis. The obtained SOM time series was
191 processed with TIMESAT software, which was developed to explore time series of vegetation
192 indices with a regular cyclicality and to retrieve the phenology metrics (Jönsson and Eklundh,
193 2004; Palmer et al., 2015). TIMESAT has been successfully applied to study phytoplankton
194 phenology in diverse aquatic environments (Benzouäi et al., 2020; Palmer et al., 2015; Shi et al.,
195 2019). The characteristic time-series was low-pass filtered with a Savitzky-Golay filter (window
196 size 4) to reduce high frequency chlorophyll variations. The start-end season methodology used
197 for our data, was the common definition of the start bloom event when Chl-a concentration rise
198 above background median concentration plus a percentage oscillating between 5 to 20 %
199 depending on the phytoplankton biomass of the region (Recault et al., 2012; Zoljoodi et al.,
200 2022). Since in our case the Chl-a concentration is relatively high (0.1 - 14 mg m⁻³) and we
201 wanted to avoid small peaks, we chose the 20 % above the median to identify the start and the
202 end of the bloom season. Four essential indices proposed by Recault et al. (2012) were used to
203 characterize phytoplankton phenology; the timing of the main bloom initiation (b_i), the peak
204 intensity (p_k), the timing of main bloom period termination (b_e) and the bloom duration. The
205 same indices were used when a secondary bloom was observed.

206 2.4 Trend analysis

207 Census X-13 seasonally adjusted methodology U.S. Census Bureau (2017) was used to remove
208 seasonality from the characteristic Chl-a time series of each biogeographical region. The Census
209 X-13 is an improved version of Census X-11, whose application to time-series analysis of

210 satellite ocean color data has been extensively documented (Delgado et al., 2015; Salgado-
 211 Hernanz et al., 2019; Vantrepotte and Mélin, 2009). The method is based on the iterative
 212 bandpass- filtering procedure that allows for the definition of a non-periodical seasonal term, in
 213 order to specifically assess the inter-annual variation in the time series seasonality (in terms of
 214 period and amplitude). The relative part of the variance of the components is estimated for each
 215 grid point, to identify the spatial patterns of the temporal variability in the series. This method
 216 aims at decomposing a time series $X(t)$ (i.e. Chl-a, phenological metrics, environmental forcing
 217 parameters derived from each biogeographical region) into three additive components: $S(t)$, the
 218 seasonal signal, $T(t)$, the trend cycle, and $I(t)$, the irregular or residual signal (Shiskin, 1978;
 219 Vantrepotte and Mélin, 2009).

220 Three successive steps are applied to decompose the time series. First, an estimation of the trend-
 221 cycle component was obtained from the annual-centred running average, and a seasonal running
 222 mean was subsequently applied to the trend series to acquire the seasonal component. Then, the
 223 series were normalized by subtracting the annual-centred running mean and the revised estimates
 224 are obtained, applying a Henderson filter of weight to the seasonal adjusted series. Finally,
 225 estimates of the trend and irregular component were calculated, repeating the application of the
 226 seasonal running mean and the Henderson filter on the revised trend adjusted series (Vantrepotte
 227 and Mélin, 2009).

228 Trends on the $T(t)$ component of Chl-a, SST, MLD, SSS and on the yearly phenological
 229 estimates (b_i , p_k , b_e and b_d) were calculated for each biogeographical region. In order to detect
 230 trends and to check its consistency we employ the Sens's method and the non-parametric
 231 seasonal Kendall statistics technique, allowing to accept or reject the presence of significant
 232 monotonic long-term change in the time series obtained from the Census X-13 method. The test
 233 relies on the computation of a suite of Mann-Kendall statistics applied monthly which finally is
 234 combined to detect the presence of long-term monotonic changes in the original time series
 235 (Vantrepotte and Mélin, 2011). The amplitude of the changes was assessed using the non-
 236 parametric Sen's slope estimator expressed in $\text{mg m}^{-3} \text{decade}^{-1}$ (Chl-a, p_k), days decade^{-1} (b_i , b_e
 237 and b_d), m decade^{-1} (MLD) and Celsius degrees decade^{-1} (SST) (Gilbert, 1987; Ibañez and
 238 Conversi, 2002).

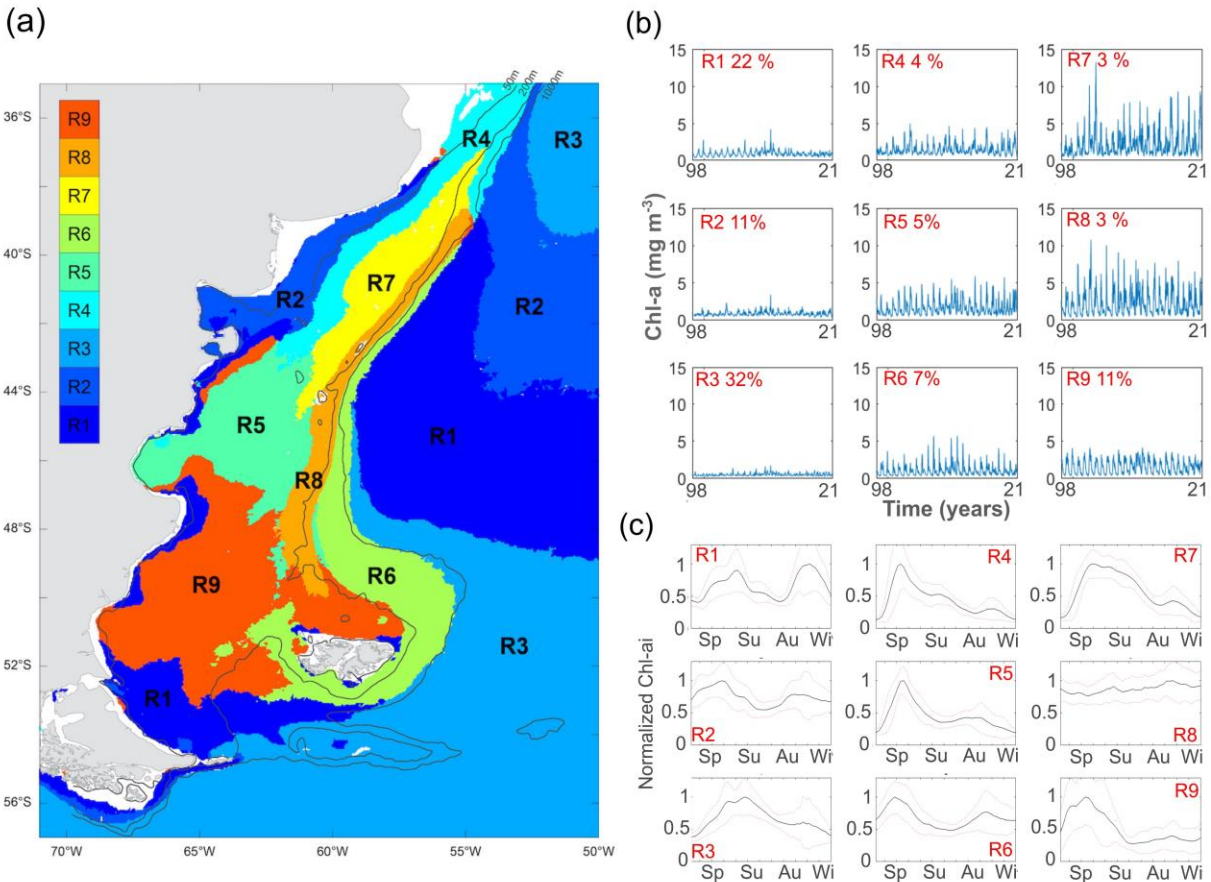
239 **3 Results**

240 **3.1 Biogeographical regionalization**

241 The 9 biogeographical regions and their corresponding characteristic temporal patterns and
 242 climatology obtained from the SOM analysis are shown in Fig. 2. The patterns are topologically
 243 ordered according to the mean value and variance. For instance, patterns with large variability
 244 and higher mean values of Chl-a concentration are located at the top-right corner of neural
 245 network, whereas those with low variability and low mean Chl-a concentrations, are located
 246 around the bottom-left corner.

247 The less productive regions (R1, R2, and R3) jointly comprise 66 % of the study area and mainly
 248 represent oceanic waters off the shelf. R3 is characterized by the lowest mean Chl-a
 249 concentration and variability of the whole study area ($0.41 \pm 0.18 \text{ mg m}^{-3}$) and includes the
 250 southern section of the study area where the Antarctic Circumpolar Current flows through the

251 Drake Passage and the Burdwood Bank. R1 is the second largest region, extending over 22 % of
 252 the study area. Mean Chl-a concentration in this region is twofold that in R1 ($0.83 \pm 0.36 \text{ mg m}^{-3}$)
 253 ³). Most of the coastal Patagonian tidal fronts, from the southern portion of San Matías Gulf until
 254 Grande Bay (southern margin of Argentina) lie within R1, as well as the northern retroflexion of
 255 Malvinas Current (MC; Fig.1). R2 corresponds to the northern inner shelf waters of the study
 256 area (El Rincón and Norpatagonian Gulfs) and to the oceanic waters located outside the shelf
 257 break northern 44° S ($0.74 \pm 0.29 \text{ mg m}^{-3}$), where the retroflexion of Brazilian Current is located
 258 (R1).



259

260 **Figure 2.** (a) Biogeographical classification Chl-a depicted from the 3 x 3 Self-Organizing Map
 261 (SOM) classification. (b) Characteristic Chl-a temporal patterns obtained from SOM
 262 computation. Inset number in red indicate the percentage of pixels clustered in each neuron. (c)
 263 Normalized climatology of the Chl-a temporal patterns. The black line stands for the mean
 264 values and the red-dashed line for the standard deviation. Sp=Spring, Su=Summer, Au=Autumn,
 265 Wi=Winter.

266 R4 and R5 represent transition regions between the open ocean waters and the highly productive
 267 regions over the southern shelf and shelf break. R4 is geographically located in the mid-shelf
 268 waters of Northern PCS. AS compared with the previous described regions, the mean value of

269 Chl-a concentration and variability are higher ($1.37 \pm 0.7 \text{ mg m}^{-3}$). Region R5 highly productive
 270 region ($1.52 \pm 0.97 \text{ mg m}^{-3}$) encompasses the San Jorge Gulf and La Isla Escondida area.

271 Regions characterized by patterns shown in the upper right corner of the neural network (R7, R8
 272 and R6, Fig.2b-c) represent the main hot spots of primary production in the Southwestern
 273 Atlantic Ocean, with chlorophyll-a concentrations exceeding in some cases 10 mg m^{-3} . The SOM
 274 analysis identifies three distinct subzones in this frontal area. Region 7 represents the north-
 275 western section of the SBF, between 37 and 44°S and located in the mid-shelf/outer-shelf,
 276 within the Argentinean Continental waters ($2.08 \pm 1.7 \text{ mg m}^{-3}$). R8 spans along the shelf-break,
 277 between $\sim 38^\circ$ and 49°S , with outstanding mean Chl-a concentrations ($2.13 \pm 1.65 \text{ mg m}^{-3}$).
 278 Finally, R6 extends between the 200 and 1000 m isobath, from 40°S to the north-western border
 279 of the Malvinas Islands. This region exhibits mean values of Chl-a comparable to R1, R2 and R3
 280 but higher variability ($0.92 \pm 0.75 \text{ mg m}^{-3}$).

281 Finally, R9 presents some similarities to R6, according to topological ordering of SOM. This
 282 region encompasses the Patagonian cold estuarine zone, off the coast of southern Patagonia,
 283 characterized by relatively high mean values and variability of Chl-a concentration ($1.4 \pm 0.9 \text{ mg}$
 284 m^{-3}). R9 extends from the outer region of the Peninsula Valdez front to the northern area of the
 285 Malvinas Islands, where it overlaps with the southern boundary of the SBF.

286 3.2 Phytoplankton phenology

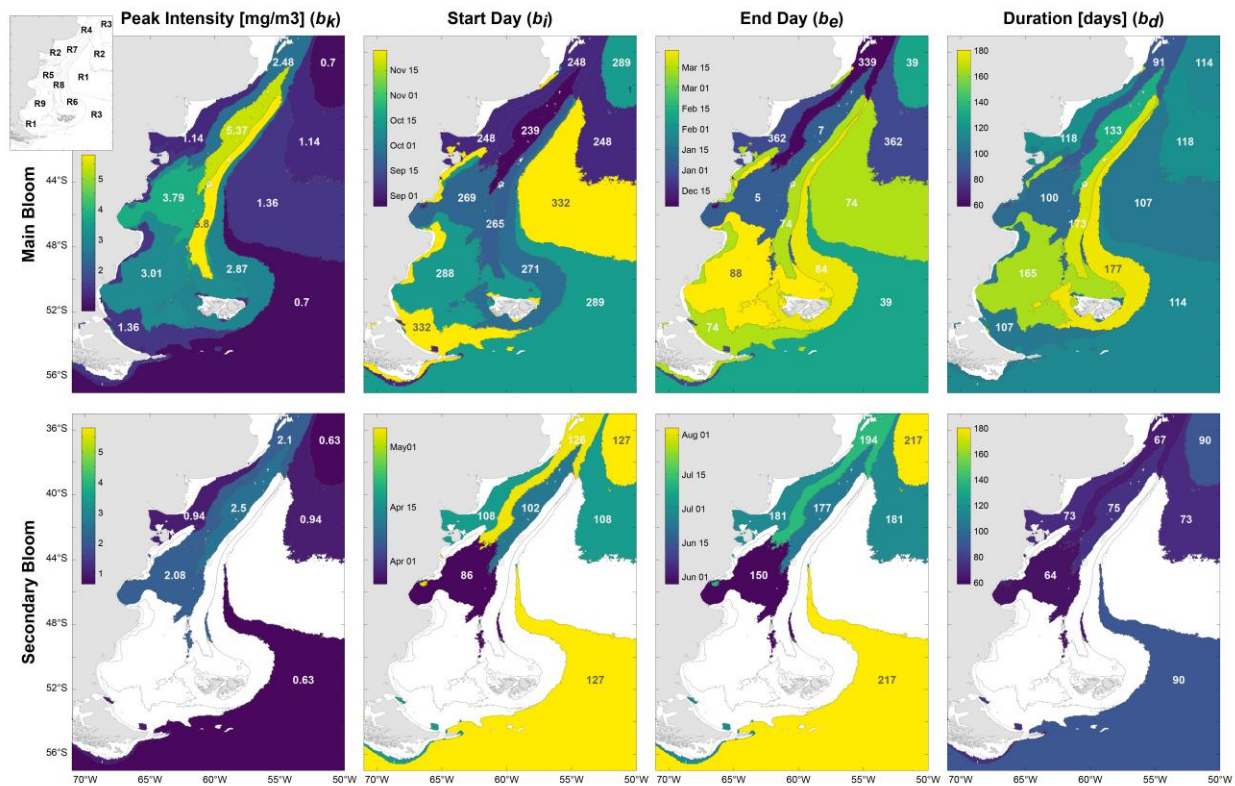
287 Phytoplankton phenology indexes are displayed in Fig.3. All regions present a main seasonal
 288 bloom in austral spring (Sep – Dec). Additionally, some regions show a secondary peak in
 289 austral autumn (Mar– Jun; Fig.3). It is worth mention that bloom detection was based in
 290 threshold values, and for some regions there were calendar years in which blooms were not
 291 detected. This was more common for the secondary bloom, which occurred in 33-87 % of the
 292 years depending on the region (supplementary material, Table S1-S2).

293 Although R3 presents relatively low Chl-a values, two blooms were identified, one in spring-
 294 summer (16^{th} Oct– 8^{th} Feb) with mean bk of 0.7 mg m^{-3} , and a secondary bloom in autumn-
 295 winter ($b_k = 0.63 \text{ mg m}^{-3}$; 7^{th} May – 5^{th} Aug). Also, R2 is characterized by two blooms with
 296 similar intensity, one in spring ($b_k = 1.14 \text{ mg m}^{-3}$; 5^{th} Sep – 28^{th} Dec) and one in autumn (b_k
 297 $= 0.94 \text{ mg m}^{-3}$; 18^{th} Apr – 30^{th} Jun). Frontal zones in R1 present a semi-annual cycle, more
 298 productive in late spring-summer, with a bloom starting by the end of November (28^{th}) and
 299 spanning for 107 days with a peak intensity of 1.36 mg m^{-3} .

300 The seasonal pattern of Patagonian temperate fronts in R5 agrees with the canonical cycles of
 301 temperate seas, where the chlorophyll maxima occurs when the water column stabilizes in early
 302 spring (26^{th} Sept – 5^{th} Jan) and a secondary bloom that takes place during fall (27^{th} Mar– 30^{th}
 303 May). The mean bk in spring is one of the highest blooms among all inferred SOM regions, 3.79
 304 mg m^{-3} . Similarly, maximum phytoplankton concentrations at R4 starts in early-spring ($b_i = 27^{\text{th}}$
 305 Aug) and spans for 91 days reaching a bk of 2.48 mg m^{-3} . During fall, the peak is shorter and
 306 weaker, as revealed by b_d and b_k values (6^{th} May – 13^{th} Jul, 2.1 mg m^{-3}).

307 In the north-western section of the shelf break (R7), the main bloom starts in early-spring ($b_i =$
 308 27^{th} Aug) and spans until the beginning of summer ($b_e = 7^{\text{th}}$ Jan), with a mean peak intensity of

309 5.37 mg m⁻³. With a lower probability of occurrence (33 % of the calendar years), the second
 310 bloom starts in autumn ($b_i = 12^{\text{th}}$ Apr) and it extends for 75 days, with an intensity of 2.5 mg m⁻³
 311 ³. In R8 and R6, corresponding to the location of the shelf-break, the bloom is registered as a
 312 single and extended spring-summer bloom ($b_d = 173 - 177$ days) starting by the end of
 313 September, with marked b_k differences (5.8 mg m⁻³ and 2.87 mg m⁻³, respectively). The
 314 estuarine cold fronts of PCS (R9) also are highly productive in spring and summer ($b_i = 15^{\text{th}}$ Oct;
 315 $b_e = 29^{\text{th}}$ Mar; $b_k = 3.01$ mg m⁻³).



316

317 **Figure 3.** Climatology of the main (upper panel) and secondary (lower panel) bloom
 318 phenological indices. The b_i and b_e dates are expressed in Julian days. b_d is expressed in days and
 319 the b_k in mg Chl-a m⁻³ (Standard deviation and significance values are showed in Table S1 of
 320 Supplementary material).

321

3.3 Trends in environmental variables, Chl-a and phytoplankton phenology

322 A positive significant trend of SST was observed in most of the biogeographical regions, with
 323 increases ranging between 0.07 ± 0.02 to 0.26 ± 0.03 °C decade⁻¹ (Table 1). Most dramatical
 324 changes (> 0.2 °C decade⁻¹) occur in R2, whereas trends in the rest of the regions average $0.07 \pm$
 325 0.04 °C decade⁻¹. A lower negative significant trend was observed on the rest of the regions, with
 326 higher negative values on R8 and R6 (Malvinas Current; $< -0.15 \pm 0.03$ °C decade⁻¹, Table 1).
 327 Even trends in MLD were more geographically variable, a significant negative trend was
 328 observed in most of the regions. Largest MLD reduction ($< -2.4 \pm 0.16$ m decade⁻¹, Table 1) was
 329 restricted to the area covered by R5, R7 and R8. Less productive regions (R1, R2, R3) did not
 330 present significant MLD trends. Likewise, Sea Surface Salinity (SSS) showed low or not

331 significant trends in these regions. Conversely, salinity declines were observed over the highly
 332 productive shelf regions (-0.19 ± 0.04 decade⁻¹; R4, R5, R7, R9; Table 1).

333 As shown in Fig.4, with the exception of R1, all regions display a significant positive trend in
 334 Chl-a, ranging between 0.03 ± 0.003 at R3 and 0.42 ± 0.04 mg m⁻³ decade⁻¹ at R7. Regions in
 335 the shelf break area, in particular the northern transitional area (R7), showed the highest
 336 increases, where the peak intensity of the spring bloom showed a significant rise up to 1.4 ± 0.04
 337 mg m⁻³ decade⁻¹ (Fig.5). Also, the Patagonian temperate frontal region (R5) presents a significant
 338 Chl-a increase of 0.13 ± 0.001 mg m⁻³ decade⁻¹.

	SST		MLD		SSS	
	Trend	p	Trend	p	Trend	p
R1	0.13±0.02	<0.05	-0.48	0.2	-0.04±0.004	<0.05
R2	0.26±0.02	<0.05	-0.43	0.28	-0.02	0.37
R3	-0.06±0.01	<0.05	-0.35	0.71	-0.02	0.06
R4	0.09	0.07	-1.52±0.12	<0.05	-0.26±0.01	<0.05
R5	0.08±0.02	<0.05	-2.49±0.17	<0.05	-0.19±0.008	<0.05
R6	-0.15±0.02	<0.05	1.8±0.46	<0.05	-0.08±0.008	<0.05
R7	0.08±0.02	<0.05	-3.36±0.13	<0.05	-0.18±0.004	<0.05
R8	-0.09±0.02	<0.05	-3.14±0.19	<0.05	-0.12±0.003	<0.05
R9	-0.07	0.05	-1.5±0.23	<0.05	-0.15±0.005	<0.05

339 **Table 1.** Trends of SST (°C decade⁻¹), MLD (m decade⁻¹) and SSS (decade⁻¹) for each region
 340 defined by SOM analysis (See Fig. 2). Statistically significant trends are highlighted ($p < 0.05$).

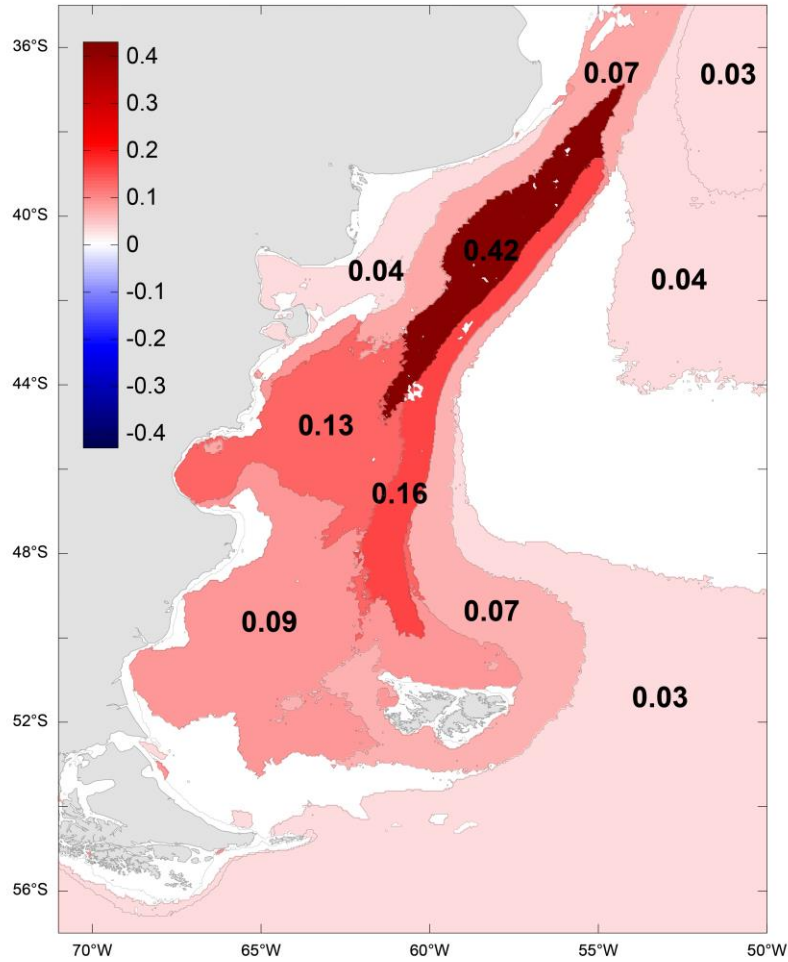
341 Significant trends for the main phenological indices are presented in Fig. 5, considering main and
 342 the secondary blooms. The spring-summer bloom starts earlier in R1 ($b_i = 28 \pm 4$ days decade⁻¹)
 343 and the bloom duration increases ($b_d = 41 \pm 11$ days). Most changes were observed in the
 344 secondary blooms of regions within the SAO (R2, R3, R4, R5, R7). The number of autumn
 345 blooms in the 24-years period was variable depending on the region considered, but in most
 346 regions there was an increasing probability for a second bloom to occur (R2, R3, R4, R5, Table
 347 S2 of Supplementary material). Furthermore, three of the five regions presented at least one
 348 significant change in the phenology estimates (R2, R3, R5). R5 b_k increase 0.38 ± 0.08 mg m⁻³
 349 decade⁻¹, as well as the starting day delayed ($b_i = 24 \pm 6$ days decade⁻¹). Also, Region 2
 350 registered a delay of the b_i , besides a delay of the bloom termination ($b_e = 34 \pm 4$ days decade⁻¹;
 351 Fig.5). Finally, in R3 the autumn bloom slightly increases the peak intensity (0.09 ± 0.04 mg m⁻³
 352 decade⁻¹), starts earlier and ends later, lengthening the bloom duration in 25 ± 5 days decade⁻¹.

353 4 Discussion

354 4.1 Biogeographical regionalization and phenological characterization

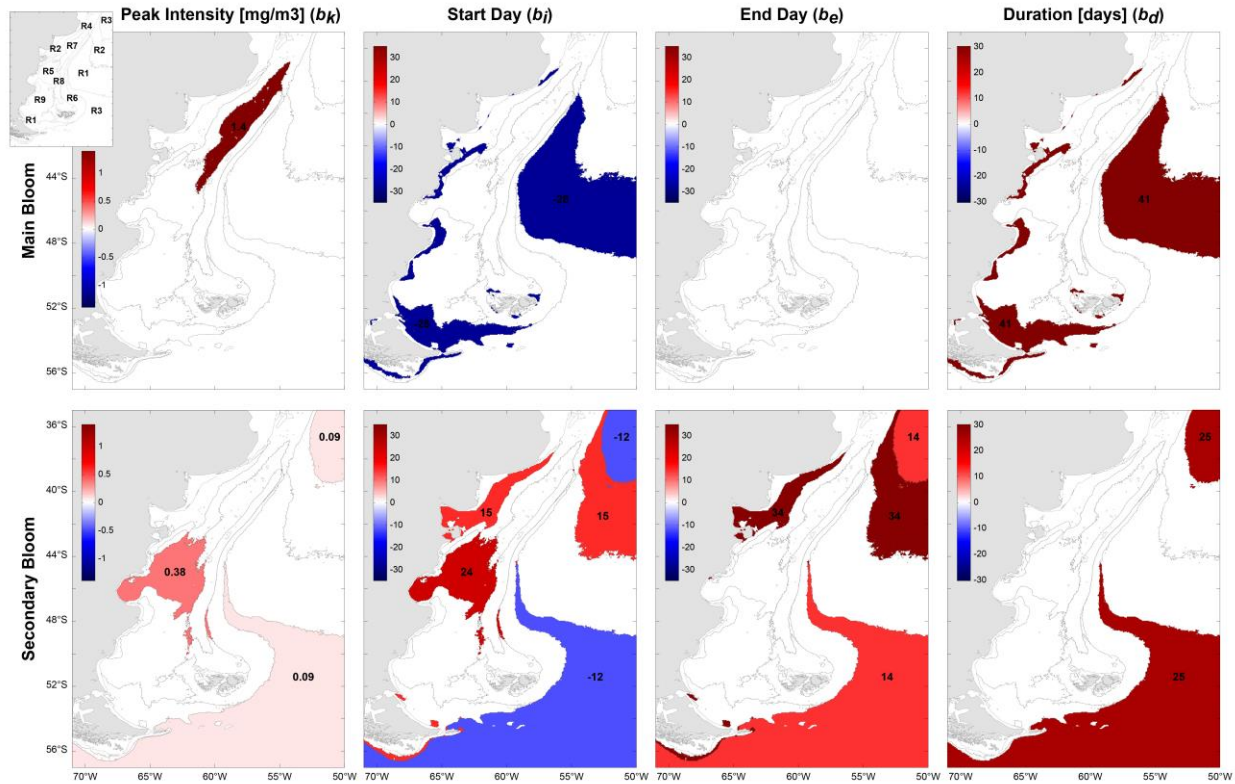
355 An objective regionalization of the SAO has been proposed based on artificial neural networks
 356 applied to satellite Chl-a data. We have identified consistent biogeographical regions that
 357 correspond to different sub-basins characterized with distinct hydrodynamical, bathymetric or
 358 ecological conditions. Two previous supervised and non-supervised regionalization based on
 359 Chl-a, SST and SST gradients has been performed for the north-eastern part of the study area

360 (R1, R2, R3), but with 6-years data and lower spatial resolution (9 km) which resulted in 8 and
 361 12 classes (Saraceno et al., 2005-2006, respectively). Our outcome in that area mostly coincides



362

363 **Figure 4.** 24-years statistically Significant Trends of Chl-a concentration ($p < 0.05$) in the
 364 biogeographical regions of the Southern Atlantic Ocean ($\text{mg m}^{-3} \text{ decade}^{-1}$).



365

366 **Figure 5.** Trends of main and secondary phenological indices. b_k is presented in $\text{mg m}^{-3} \text{decade}^{-1}$
 367 and b_i , b_e and b_d in days decade^{-1} . Only the regions painted are statistically significant ($p < 0.05$).

368 with the results presented by Saraceno et al. (2005-2006), where the R3, R2 and R1 are also
 369 separated for representing the AO off the Patagonian Shelf.

370 The biggest depicted region from SOM (R3) includes oligotrophic oceanic waters outside the
 371 PCS as well as the Burwood Bank, an undersea bank that forms a barrier to the northward flow
 372 of the Antarctic Circumpolar Current and generates conditions that sustain important fisheries
 373 (García Alonso et al., 2018; Casarsa et al., 2019). Although it is recognized as a highly
 374 productive area (Fig.1), it presents relatively low Chl-a concentrations and phytoplankton
 375 biomass. It was suggested that blooms in this area would develop deeper in the water column,
 376 due to the presence of fast ocean currents advecting nutrients to the subpolar basin (Matano et
 377 al., 2019; Guinder et al., 2020). Two of the largest regions (R1 and R2), which are characterized
 378 with relatively low Chl-a concentration, include areas of oceanic and coastal waters with the
 379 same Chl-a temporal variability patterns, but with different mechanisms triggering the blooms.
 380 R1 includes the coastal Patagonian tidal fronts area, whose location are defined by the boundary
 381 between the stratified mid-shelf and the coastal mixed waters. Stratification in the mid-shelf sets
 382 during spring-summer is due to the increase in solar radiation, and seasonal fronts develop at the
 383 boundary between stratified conditions and tidally mixed coastal waters (Acha et al., 2004). R2,
 384 close to the coast, includes the Norpatagonian Gulfs and El Rincón waters (inner shelf).
 385 Phenological patterns described for this region agree with previous findings in San Matías Gulf,
 386 two phytoplankton biomass patterns were observed: one representing the inner waters, where
 387 two blooms were described (autumn-spring), associated with seasonal stratification of the water

388 column in spring, and bloom decay through summer as a result of nutrient limitation and a
389 maximum in autumn due to a high concentration of nutrients linked to the beginning of the
390 vertical homogenization of the water column; and the mid-shelf waters pattern, where one main
391 bloom with low variability related to the vertical mixing in water column in the coastal areas and
392 light and nitrate availability, developed in late-autumn in the N section and in spring in the S
393 section (Williams et al., 2021). Meanwhile, El Rincón even presents a salinity and a thermal
394 front generated by bathymetry changes and dilution effects, combined with the northern
395 advection of San Matías Gulf waters (Lucas et al., 2005; Rivas and Pisoni, 2010), no clear
396 seasonality of in situ phytoplankton concentration has been reported in this area (Delgado et al.,
397 2015). Both regions, R1 and R2, cover together the retroreflection of BC, which is one of the
398 branches of the SAC, is an eastward conduit of biogenic material on the outer shelf (Signorini et
399 al., 2009). The division in two regions resulted from the SOM is in concordance with Saraceno et
400 al. (2005) where also Chl-a concentration differences was observed. Special attention should be
401 given to the variability and trends of this area, since is a source of productivity for the rest of the
402 South Atlantic Ocean.

403 The physical mechanisms that trigger the temperate PCS mid-shelf bloom, that covers 9 % of the
404 study area (R5 and R4), are the same, but the blooms result in different bk, bi and be and SOM
405 could successfully separate both. These areas allow for the development of economically
406 important fisheries: The Patagonian temperate fronts (R5) are an important spawning and nursery
407 area of several commercial species (e.g. Argentine red shrimp, Argentine hake, southern king
408 crab, Segura et al. 2021), and R4 is one of the main spring spawning and nursery area for the
409 northern population of *E. anchoita* (Marrari et al., 2013). The seasonal pattern of these regions
410 agrees with the canonical cycle of temperate seas, where the chlorophyll maxima is associated
411 with the onset of stratification in spring, and a second smaller peak during fall, when the
412 thermocline weakens and deeper nutrient rich waters entrain the surface layer (Carreto et al.,
413 1995; Akselman, 1996; Rivas and Beier, 1990). In R5 both blooms start one month later
414 compared to R4, probably because of later light availability and stratification of the water
415 column for the latitudinal location of the area (southern). The strong peak of R5 is consistent
416 with previous observations in the San Jorge Gulf, where bloom intensity reached $\sim 9 \text{ mg m}^{-3}$
417 (2008) and high values ($> 1.5 \text{ mg m}^{-3}$) persisted during summer (Fig.2, Segura et al., 2021). The
418 northern Patagonian mid-shelf front (R4) is a $\sim 80 \text{ km}$ band of high chlorophyll concentration
419 offshore of the 50 m. During spring-summer the front is developed, by the vertical stratification
420 of waters located $\sim 80 \text{ m}$ offshore with a thermocline overlying colder nutrient-rich waters (MC),
421 separating the vertically mixed nutrient-poor coastal waters (R2) (Lucas et al., 2005; Martos and
422 Piccolo, 1988). The end of the bloom in the beginning of summer due to the combined effect of
423 nutrient depletion during the preceding bloom and the development of strong thermal
424 stratification (Carreto et al., 1995).

425 The shelf-break (SBF) front is a thermohaline permanent front, that broadens and intensifies in
426 spring and summer (Rivas and Pisoni, 2010), delimiting the boundary between the low salinity
427 shelf waters and the colder, saltier and nutrient rich waters of the Malvinas Current (Romero et
428 al., 2006). The persistence of the shelf break bloom is sustained by permanent upwelling of
429 nutrient rich waters (MC) into the euphotic zone caused by the interaction of the MC with
430 bathymetry (Matano and Palma, 2008). Within the Shelf-Break, the bioregionalization allowed
431 for the identification of three different regions, improving our understanding of their triggering
432 mechanisms and their sensibility to environmental forces and changes. The north of the SB (R7)

433 presents a high inter-annual temporal variability, since it may present one single spring-summer
434 bloom like the rest of SBF (R8) or a spring and autumn bloom, like the MSF (R4), depending on
435 the environmental conditions of a given year. The complex structure of the SBF in this area was
436 analysed by Franco et al. (2008), and a strong Chl-a gradient was described, perpendicular to the
437 front, possibly caused by multiple branches of Malvinas Current. Between the 100 and 1000 m
438 isobath, from 40 °S till the northern-west border of Malvinas Islands, is located R6, a transitional
439 zone between the SBF and the AO. This portion of the SBF is mainly separated by the SOM not
440 because the timing of the bloom (similar to R8), but because the mean values of Chl-a and bk are
441 considerably half lower than the other two regions.

442 Region R9, encompassing the Patagonian cold estuarine zone, is characterized by a semi-annual
443 cycle. This region is extended from the outer region of the Peninsula Valdez front up to the
444 northern area of Malvinas Islands, overlapping with the south-western portion of the SBF. The
445 water masses located north of the Drake Passage are diluted due to low salinity waters coming
446 from SE Pacific through the Le Marie Strait and the continental run-off of Patagonian main
447 rivers (Lusquiños and Valdéz, 1971; Dai and Trenberth, 2002). The diluted plume, mixed by
448 strong tides and winds (westerlies) is traced till the 100 m isobath and southern San Jorge Gulf
449 (Acha et al., 2004).

450 4.2 Environmental, phytoplankton biomass and phenology trends in the SAO

451 Western boundary currents are expected to progressively warm as a result of the poleward
452 migration of the subtropical ocean gyres. Indeed, the Brazil Current has been identified as one of
453 the most extensive and intense surface warming hotspots globe wide (Hobday and Pecl, 2014).
454 Our results (see R7 and R2 in Table 1) are consistent with recent studies reporting a warming
455 trend of 0.4° decade⁻¹ in the Brazil-Malvinas Confluence and the SBF (e.g. Franco et al., 2020,
456 2022) as well as in the San Matías and Nuevo Gulfs (Williams and Nocera, 2023). Also, a higher
457 water temperature associated with global warming is predicted over the shelf where the heat
458 exchange between the sea and the atmosphere is strong (Leyba et al., 2019), and this is in
459 agreement with the most pronounced warming trend found in our study.

460 The depth and properties of the MLD depend on ocean-atmosphere exchanges which are
461 strongly influenced by climate variability (Sallée et al., 2010). Our results indicate consistent
462 shallowing of the MLD (Table 1) and agree with a previous study which address a shoaling trend
463 of the MLD in the Patagonian Shelf (Franco et al., 2023; Williams and Nocera, 2023), with the
464 highest values in the north-western portion of the mid-shelf and the shelf-break (Franco et al.,
465 2022), also in line with the highest trend find in R7 of this study. In the Patagonian shelf the
466 MLD depends mainly on the thermal stratification (Signorini et al., 2006); thus, the increase in
467 SST due to global warming is expected to produce longer periods of shallower MLD (typical of
468 spring and summer), resulting in the negative observed trend.

469 Sea Surface Salinity (SSS) also presented significant changes in the studied period in most of the
470 regions. All trends are negative, with higher impact in region 4, 5 and 7. The dilution of the
471 northern Patagonian shelf (above $\sim -42^{\circ}$) depends mainly on the discharge of major rivers (La
472 Plata, Negro, and Colorado rivers), which are known to present high variability associated to
473 climate variability in general and ENSO events in particular (Acha et al., 2008; Delgado et al.,
474 2015), thus the increase of extreme events associated to climate change (Dai et al., 1997; Hansen

475 et al., 2006) might be affecting the amount of continental runoff to shelf waters (Pasquini et al.,
476 2010). Possible R2 does not present a negative significant trend, because the salinity on that area
477 also depend on the saline water plume coming from the San Matías Gulf waters which depend on
478 the evaporation over the precipitation balance on the gulf (Lucas et al., 2005). The southern shelf
479 (R1, R9, R5) is diluted mainly for waters coming from the SE Pacific, resulted from glaciers
480 melting and heavy rainfall (> 2000 mm annual), entering in the Argentinean territory through Le
481 Marie strait, and the Santa Cruz River (Luzquiños and Valdéz, 1971; Dai and Trenberth, 2002).

482 Although the temporal stability of satellite products based on merging data from different
483 sensors, as Globcolour, should be carefully analyzed (Garnesson et al., 2019), in particular for
484 trend computations, our results are consistent with previous positive phytoplankton biomass
485 trends observed in the study area using two sensors (SeaWiFS and MODIS-Aqua: Marrari et al.,
486 2017), or only one sensor (MODIS-Aqua: Franco et al., 2020 and Williams et al., 2023;
487 SeaWiFS: Vantrepotte and Mélin, 2009). The significant trends in Chl-a concentration and
488 phenology indexes presented in this study may be influencing the marine system functioning as
489 they describe changes at the base of the food web, and several factors could be leading these
490 strong trends. In line with our results, previous studies addressed the increasing trend of Chl-a
491 concentration covering then entire Patagonian Shelf or the SBF (Marrari et al., 2017; Franco et
492 al., 2022), but none studies of trends of phenological indices was performed before. Franco et al.
493 (2022) suggested an intensification of the SBF results from a cooling of the MC (SST negative
494 trend in R8, Table 1) and a warming of the adjacent shelf (SST positive trend in R7, Table 1). It
495 combines with the intensification of winds parallel to the front (Risaro et al., 2022) that may
496 enhance the turbulent mixing and increase the upwelling on the onshore side of the front (Franco
497 et al., 2022). All these changes combined would benefit phytoplankton and increase their
498 productivity. On the other hand, we hypothesized that since nutrients are not a limiting factor in
499 the SBF (e.g. Matano and Palma, 2008; Valla and Piola, 2015), a shallower MLD (~ -3.3 m
500 decade⁻¹) might benefit and extended bloom since it enhances the light availability (Franco et
501 al., 2022). Also, there is a succession of phytoplankton groups in the SBF. Typically, a bloom is
502 diatom-dominated in early spring (MLD 40-80 m, nutrient-rich waters), and after nutrient
503 depletion, coccolithophores (*Emiliana huxleyi*) dominate in summer when the MLD reaches its
504 minimum (18 m) (Signorini et al., 2009). Thus, these smaller species could benefit from the
505 negative trend of the MLD. The increasing trend in the Chl-a concentration may be due, not only
506 to a higher phytoplankton biomass, but also to a change in dominance to coccolithophores, as
507 their blooms produce a high concentration of detached coccoliths (plates of calcium carbonate)
508 characterized by a high reflectance (Holligan et al., 1993).

509 The most sticking changes observed in this study are related to the secondary bloom that
510 appeared in most regions within the PCS. In R2 and R5, a delay in the start of the autumn bloom
511 of 15 and 24 days, respectively was observed. Secondary blooms occur in austral autumn (Apr-
512 May) generally associated with the weakening of the thermocline and the mixing of the water
513 column, supplying nutrient rich bottom waters to the euphotic zone (Akselman, 1996; Rivas and
514 Beier, 1990). The significant warming trend of SST would sustain stratification for a longer
515 period, thus delaying the secondary bloom initialization. Many long-term phytoplankton studies
516 have noted that the timing of the spring bloom is rather constant, occurring approximately the
517 same time each year under highly variable environmental conditions (Eilertsen and Wyatt, 2000),
518 since light is the limitation factor. But, other blooms as may not only be responding
519 physiologically to temperature, they may also respond to temperature indirectly if climate

520 warming enhances stratified conditions and/or if these conditions appeared earlier (Edwards and
521 Richardson, 2004) or later in the season in the PCS.

522 **5 Conclusions**

523 The bioregionalization conducted in the present study allowed the identification, of 9 meaningful
524 areas showing coherent patterns of Chl-a dynamics which are consistent with the oceanographic
525 and biogeochemical characteristics of the Southwestern Atlantic Ocean. The regions permitted to
526 evaluate the areas which have different phenological estimates, mean Chl-a concentration and
527 with different mechanisms triggering the blooms. The regionalization facilitates and improve the
528 analysis of environmental and biological changes in this extensive and highly complex region.
529 The phenology of phytoplankton blooms in these coherent regions have been presented, showing
530 a main seasonal bloom in austral spring (Sep – Dec) in all of them with different timing and
531 intensity, and a secondary peak in austral autumn (Mar– Jun) in some regions, depending on the
532 year.

533 Significant positive trends in total biomass have been registered in most of regions, with higher
534 Chl-a concentration increase in the shelf-break, especially in the northern area (R7). The
535 remarkable increment in Chl-a concentration of R7 is suggested to be attributed to frontal
536 intensification because of the SST warming, the MLD shoaling and the resulted possible benefit
537 of coccolithophores blooms. In addition, changes in the frequency (more frequent), timing
538 (earlier), and intensity (more intense) of the secondary (autumn) blooms are registered in regions
539 corresponding to the Patagonian temperate front (R5) and the Norpatagonian Gulfs and El
540 Rincón waters (R2). It is suggested that the significant warming trend of SST would sustain
541 stratification for a longer period, thus delaying the secondary bloom initialization This bloom
542 delay could drastically impact on the survival of fish larvae and recruitment as many of the
543 regions are spawning and/or nurse areas, i.e. R2, R4 and R5 (Cushing, 1990). In temperate and
544 high-latitude pelagic ecosystems, may be particularly vulnerable to phenological changes caused
545 by climatic warming, as observed in the SAO. Recruitment success of higher trophic levels is
546 highly dependent on synchronization with seasonally pulsed primary production and the
547 response to regional warming varies among functional groups. Changes in any of these can lead
548 to mismatch in timing between trophic levels (Edwards and Richardson, 2004; Ji et al., 2010).

549 Although we cannot talk about climate change because our analysis is based on 24 years of data,
550 the observed changes in the main environmental conditions: ocean warming, shoaling of mixed
551 layer depth and less saline seas; are in line with worldwide trends related to climate change
552 estimates (IPCC, 2022). The variations produced by the main environmental drivers associated
553 with the climate change would possibly increase and led to unpredicted results. The depicted
554 bioregionalization and the observed variations in the phytoplankton phenology metrics will be
555 relevant to further investigate the ongoing and future changes, as well as the implications that
556 this might have on higher trophic levels and on commercial fisheries.

557 **Acknowledgments**

558 The authors would like to thank the Consejo Nacional de Investigaciones Científicas y Técnicas
559 (CONICET) for their financial support (BECA EXTERNA). This research was done in the frame

560 of I-COOP 2021 project founded by the Consejo Superior de Investigaciones Científicas and the
561 PICT2020-Serie A-02309 founded by the Agencia Nacional de Promoción de la Investigación, el
562 Desarrollo Tecnológico y la Innovación. The present research was carried out within the
563 framework of the activities of the Spanish Government through the “María de Maeztu Centre of
564 Excellence” accreditation to IMEDEA (CSIC-UIB) (CEX2021-001198-M)". I. Hernandez-
565 Carrasco acknowledges financial support from the project TRITOP (grant: UIB2021-PD06)
566 funded by University of the Balearic Islands and by FEDER(EU). V. Combes acknowledges the
567 support of NSF grants OCE-1830856, OCE-2149093, OCE-2149292, NASA award
568 80NSSC21K0559, and the support from the Spanish Ramón y Cajal Program (RYC2020-
569 029306-I) through grant AEI/UIB - 10.13039/501100011033. J.S Font-Muñoz acknowledges
570 funding by an individual postdoctoral fellowship “Margalida Comas” (PD/018/2020) from
571 Govern de les Illes Balears and Fondo Social Europeo. P. Pratolongo thanks the financial support
572 of Pampa Azul (B8). We all thank the GlobColour and Copernicus groups for the distribution of
573 satellite merged products and modeled data, respectively.

574 **Open Research**

575 The Globcolour data can be downloaded from <https://hermes.acri.fr/> and the GLORYSv12 data
576 can be downloaded from <https://data.marine.copernicus.eu>. The SOM v.2.0 MATLAB toolbox
577 can be obtained from <http://www.cis.hut.fi/somtoolbox/>; the TIMESAT software from
578 <https://web.nateko.lu.se/timesat/timesat.asp>; the Census X-13 toolbox from
579 <https://es.mathworks.com/matlabcentral/fileexchange/49120-x-13-toolbox-for-seasonal-filtering>
580 and the Sen’s slope estimator from [https://es.mathworks.com/matlabcentral/fileexchange/11190-](https://es.mathworks.com/matlabcentral/fileexchange/11190-mann-kendall-tau-b-with-sen-s-method-enhanced)
581 [mann-kendall-tau-b-with-sen-s-method-enhanced](https://es.mathworks.com/matlabcentral/fileexchange/11190-mann-kendall-tau-b-with-sen-s-method-enhanced).

582

583 **References**

- 584 Alvain, S., Moulin, C., Dandonneau, Y., & Loisel, H. (2008). Seasonal distribution and
585 succession of dominant phytoplankton groups in the global ocean: A satellite
586 view. *Global Biogeochemical Cycles*, 22(3). <https://doi.org/10.1029/2007GB003154>
- 587 Acha, E. M., Mianzan, H., Guerrero, R., Carreto, J., Giberto, D., Montoya, N., & Carignan, M.
588 (2008). An overview of physical and ecological processes in the Rio de la Plata
589 Estuary. *Continental shelf research*, 28(13), 1579-1588.
590 <https://doi.org/10.1016/j.csr.2007.01.031>, 2008
- 591 Acha, E. M., Mianzan, H. W., Guerrero, R. A., Favero, M., & Bava, J. (2004). Marine fronts at
592 the continental shelves of austral South America: physical and ecological
593 processes. *Journal of Marine systems*, 44(1-2), 83-105.
594 <https://doi.org/10.1016/j.jmarsys.2003.09.005>, 2004
- 595 Anderson, S. I., Barton, A. D., Clayton, S., Dutkiewicz, S., & Rynearson, T. A. (2021). Marine
596 phytoplankton functional types exhibit diverse responses to thermal change. *Nature*
597 *communications*, 12(1), 6413. <https://doi.org/10.1038/s41467-021-26651-8>
- 598 Armstrong, R. A., Gilbes, F., Guerrero, R., Lasta, C., Benavidez, H., & Mianzan, H. (2004).
599 Validation of SeaWiFS-derived chlorophyll for the Rio de la Plata Estuary and adjacent
600 waters. *International Journal of Remote Sensing*, 25(7-8), 1501-1505.
- 601 Artana, C., Provost, C., Lellouche, J. M., Rio, M. H., Ferrari, R., & Sennéchaël, N. (2019). The
602 Malvinas current at the confluence with the Brazil current: Inferences from 25 years of
603 Mercator ocean reanalysis. *Journal of Geophysical Research: Oceans*, 124(10), 7178-
604 7200. <https://doi.org/10.1029/2019JC015289>

- 605 Akselman, R. (1996). Estudios ecológicos en el Golfo San Jorge y adyacencias (Atlántico
606 Sudoccidental): Distribución, abundancia y variación estacional del fitoplancton en
607 relación a factores Físico-químicos y la dinámica hidrológica. Doctoral dissertation,
608 Universidad de Buenos Aires. Facultad de Ciencias Exactas y Naturales,
609 https://hdl.handle.net/20.500.12110/tesis_n2857_Akselman.
- 610 Basterretxea, G., Font-Muñoz, J. S., Salgado-Hernanz, P. M., Arrieta, J., & Hernández-Carrasco,
611 I. (2018). Patterns of chlorophyll interannual variability in Mediterranean
612 biogeographical regions. *Remote sensing of environment*, 215, 7-17.
613 <https://doi.org/10.1016/j.rse.2018.05.027>
- 614 Ben Mustapha, Z., Alvain, S., Jamet, C., Loisel, H., & Dessailly, D. (2014). Automatic
615 classification of water-leaving radiance anomalies from global SeaWiFS imagery:
616 application to the detection of phytoplankton groups in open ocean waters. *Remote
617 sensing of environment*, 146, 97-112. <https://doi.org/10.1016/j.rse.2013.08.046>
- 618 Benzouai, S., Louanchi, F., & Smara, Y. (2020). Phytoplankton phenology in algerian
619 continental shelf and slope waters using remotely sensed data. *Estuarine, Coastal and
620 Shelf Science*, 247, 107070. <https://doi.org/10.1016/j.ecss.2020.107070>
- 621 Cai, W., McPhaden, M. J., Grimm, A. M., Rodrigues, R. R., Taschetto, A. S., Garreaud, R. D., ...
622 & Vera, C. (2020). Climate impacts of the El Niño–southern oscillation on South
623 America. *Nature Reviews Earth & Environment*, 1(4), 215-231.
624 <https://doi.org/10.1038/s43017-020-0040-3>
- 625 Carreto, J., Lutz, V. A., Carignan, M. O., Colleoni, A. D. C., & De Marco, S. G. (1995).
626 Hydrography and chlorophyll a in a transect from the coast to the shelf-break in the

- 627 Argentinian Sea. *Continental Shelf Research*, 15(2-3), 315-336.
628 [https://doi.org/10.1016/0278-4343\(94\)E0001-3](https://doi.org/10.1016/0278-4343(94)E0001-3)
- 629 Casarsa, L., Diez, M. J., Madirolas, A., Cabreira, A. G., & Buratti, C. C. (2019). Morphometric
630 description of schools from two different stocks of the southernmost sprat *Sprattus*
631 *fuegensis*. *Fisheries Research*, 212, 29-34. <https://doi.org/10.1016/j.fishres.2018.12.004>
- 632 Cushing, D. H., 1990. Plankton production and year-class strength in fish populations: an update
633 of the match/mismatch hypothesis, in: *Advances in marine biology*, edited by: J.H.S.
634 Blaxter, A.J. Southward, Vol. 26, Academic Press. [https://doi.org/10.1016/S0065-](https://doi.org/10.1016/S0065-2881(08)60202-3)
635 [2881\(08\)60202-3](https://doi.org/10.1016/S0065-2881(08)60202-3)
- 636 Dai, A., Fung, I. Y., & Del Genio, A. D. (1997). Surface observed global land precipitation
637 variations during 1900–88. *Journal of climate*, 10(11), 2943-2962. [https://doi.org/](https://doi.org/10.1175/1525-7541)
638 [10.1175/1525-7541](https://doi.org/10.1175/1525-7541)
- 639 Delgado, A. L., Guinder, V. A., Dogliotti, A. I., Zapperi, G., & Pratolongo, P. D. (2019).
640 Validation of MODIS-Aqua bio-optical algorithms for phytoplankton absorption
641 coefficient measurement in optically complex waters of El Rincón
642 (Argentina). *Continental Shelf Research*, 173, 73-86.
643 <https://doi.org/10.1016/j.csr.2018.12.012>
- 644 Delgado, A. L., Loisel, H., Jamet, C., Vantrepotte, V., Perillo, G. M., & Piccolo, M. C. (2015).
645 Seasonal and inter-annual analysis of chlorophyll-a and inherent optical properties from
646 satellite observations in the inner and mid-shelves of the south of Buenos Aires Province
647 (Argentina). *Remote Sensing*, 7(9), 11821-11847. <https://doi.org/10.3390/rs70911821>
- 648 Delgado, A. L., Pratolongo, P. D., Dogliotti, A. I., Arena, M., Celleri, C., Cardona, J. E. G., &
649 Martinez, A. (2021). Evaluation of MODIS-Aqua and OLCI Chlorophyll-a products in

650 contrasting waters of the Southwestern Atlantic Ocean. *Ocean and Coastal Research*, 69.

651 <https://doi.org/10.1590/2675-2824069.20-003ald>

652 Dogliotti, A. I., Schloss, I. R., Almandoz, G. O., & Gagliardini, D. A. (2009). Evaluation of
653 SeaWiFS and MODIS chlorophyll-a products in the Argentinean Patagonian continental
654 shelf (38 S–55 S). *International Journal of Remote Sensing*, 30(1), 251-273.

655 <https://doi.org/10.1080/01431160802311133>

656 Doney, S. C., Ruckelshaus, M., Emmett Duffy, J., Barry, J. P., Chan, F., English, C. A., ... &
657 Talley, L. D. (2012). Climate change impacts on marine ecosystems. *Annual review of*
658 *marine science*, 4, 11-37. <https://doi.org/10.1146/annurev-marine-041911-111611>

659 Drévillon, M., Lellouche, J-M., Réginer, C., Garric, G., Bricaud, C., Hernandez, O., Bourdallé-
660 Badie, R., 2022. Quality information document for Global Ocean Reanalysis Products.
661 CMEMS-GLO-QUID-001-030.

662 Dutkiewicz, S., Scott, J. R., & Follows, M. J. (2013). Winners and losers: Ecological and
663 biogeochemical changes in a warming ocean. *Global Biogeochemical Cycles*, 27(2), 463-
664 477. <https://doi.org/10.1002/gbc.20042>

665 Edwards, M., & Richardson, A. J. (2004). Impact of climate change on marine pelagic
666 phenology and trophic mismatch. *Nature*, 430(7002), 881-884.

667 <https://doi.org/10.1038/nature02808>

668 Eilertsen, H. C., & Wyatt, T. (2000). Phytoplankton models and life history strategies. *South*
669 *African Journal of Marine Science*, 22(1), 323-338.

670 <https://doi.org/10.2989/025776100784125717>

- 671 Ferreira, A., Garcia, C. A., Dogliotti, A. I., & Garcia, V. M. (2013). Bio-optical characteristics of
672 the Patagonia Shelf break waters: Implications for ocean color algorithms. *Remote*
673 *sensing of environment*, 136, 416-432. <https://doi.org/10.1016/j.rse.2013.05.022>
- 674 Field, C. B., Behrenfeld, M. J., Randerson, J. T., & Falkowski, P. (1998). Primary production of
675 the biosphere: integrating terrestrial and oceanic components. *science*, 281(5374), 237-
676 240. <https://doi.org/10.1126/science.281.5374.237>
- 677 Franco, B. C., Piola, A. R., Rivas, A. L., Baldoni, A., & Pisoni, J. P. (2008). Multiple thermal
678 fronts near the Patagonian shelf break. *Geophysical Research Letters*, 35(2).
679 <https://doi.org/10.1029/2007GL032066>
- 680 Franco, B. C., Ruiz-Etcheverry, L. A., Marrari, M., Piola, A. R., & Matano, R. P. (2022).
681 Climate change impacts on the Patagonian Shelf break front. *Geophysical Research*
682 *Letters*, 49(4), e2021GL096513. <https://doi.org/10.1029/2021GL096513>
- 683 Franco, B. C., Combes, V., & González Carman, V. (2020). Subsurface ocean warming hotspots
684 and potential impacts on marine species: the southwest South Atlantic Ocean case
685 study. *Frontiers in Marine Science*, 7, 563394.
686 <https://doi.org/10.3389/fmars.2020.563394>
- 687 Friedlingstein, P., Jones, M. W., O'sullivan, M., Andrew, R. M., Hauck, J., Peters, G. P., ... &
688 Zaehle, S. (2019). Global carbon budget 2019. *Earth System Science Data*, 11(4), 1783-
689 1838. doi.org/10.5194/essd-11-1783-2019
- 690 García Alonso, V. A., Brown, D., Martín, J., Pájaro, M., & Capitano, F. L. (2018). Seasonal
691 patterns of Patagonian sprat *Sprattus fuegensis* early life stages in an open sea Sub-
692 Antarctic Marine Protected Area. *Polar Biology*, 41, 2167-2179.
693 <https://doi.org/10.1007/s00300-018-2352-z>

- 694 Garcia, V. M., Garcia, C. A., Mata, M. M., Pollery, R. C., Piola, A. R., Signorini, S. R., ... &
695 Iglesias-Rodriguez, M. D. (2008). Environmental factors controlling the phytoplankton
696 blooms at the Patagonia shelf-break in spring. *Deep Sea Research Part I: Oceanographic*
697 *Research Papers*, 55(9), 1150-1166. <https://doi.org/10.1016/j.dsr.2008.04.011>
- 698 Garnesson, P., Mangin, A., Fanton d'Andon, O., Demaria, J., & Bretagnon, M. (2019). The
699 CMEMS GlobColour chlorophyll a product based on satellite observation: Multi-sensor
700 merging and flagging strategies. *Ocean Science*, 15(3), 819-830.
- 701 Garnesson, P., Mangin, A. and Bretagnon, M.: Quality information document. CMEMS-OC-
702 QUID-009-101to104-116-118, 2.
- 703 Gilbert, R. O. (1987). *Statistical methods for environmental pollution monitoring*. John Wiley &
704 Sons.
- 705 Good, S., Fiedler, E., Mao, C., Martin, M. J., Maycock, A., Reid, R., ... & Worsfold, M. (2020).
706 The current configuration of the OSTIA system for operational production of foundation
707 sea surface temperature and ice concentration analyses. *Remote Sensing*, 12(4), 720.
- 708 Guinder, V. A., Malits, A., Ferronato, C., Krock, B., Garzón-Cardona, J., & Martínez, A. (2020).
709 Microbial plankton configuration in the epipelagic realm from the Beagle Channel to the
710 Burdwood Bank, a Marine Protected Area in Sub-Antarctic waters. *Plos one*, 15(5),
711 e0233156. <https://doi.org/10.1371/journal.pone.0233156>
- 712 Guinder, V. A., Tillmann, U., Krock, B., Delgado, A. L., Krohn, T., Garzón Cardona, J. E., ... &
713 Lara, R. (2018). Plankton multiproxy analyses in the Northern Patagonian Shelf,
714 Argentina: Community structure, phycotoxins, and characterization of toxic Alexandrium
715 strains. *Frontiers in Marine Science*, 5, 394. <https://doi.org/10.3389/fmars.2018.00394>

- 716 Hansen, J., Sato, M., Ruedy, R., Lo, K., Lea, D. W., & Medina-Elizade, M. (2006). Global
717 temperature change. *Proceedings of the National Academy of Sciences*, 103(39), 14288-
718 14293. <https://doi.org/10.1073/pnas.0606291103>
- 719 Hernández-Carrasco, I., & Orfila, A. (2018). The Role of an Intense Front on the Connectivity of
720 the Western Mediterranean Sea: The Cartagena-Tenes Front. *Journal of Geophysical
721 Research: Oceans*, 123(6), 4398-4422. <https://doi.org/10.1029/2017JC013613>
- 722 Hobday, A. J., & Pecl, G. T. (2014). Identification of global marine hotspots: sentinels for
723 change and vanguards for adaptation action. *Reviews in Fish Biology and Fisheries*, 24,
724 415-425. <https://doi.org/10.1007/s11160-013-9326-6>
- 725 Holligan, P. M., Fernández, E., Aiken, J., Balch, W. M., Boyd, P., Burkill, P. H., ... & van der
726 Wal, P. (1993). A biogeochemical study of the coccolithophore, *Emiliana huxleyi*, in the
727 North Atlantic. *Global biogeochemical cycles*, 7(4), 879-900.
728 <https://doi.org/10.1029/93GB01731>
- 729 Ibanez, F., & Conversi, A. (2002). Prediction of missing values and detection of ‘exceptional
730 events’ in a chronological planktonic series: a single algorithm. *Ecological
731 Modelling*, 154(1-2), 9-23. [https://doi.org/10.1016/S0304-3800\(02\)00033-9](https://doi.org/10.1016/S0304-3800(02)00033-9)
- 732 IPCC, 2022: Climate Change 2022: Impacts, Adaptation, and Vulnerability. Contribution of
733 Working Group II to the Sixth Assessment Report of the Intergovernmental Panel on
734 Climate Change. H.-O. Pörtner, D.C. Roberts, M. Tignor, E.S. Poloczanska, K.
735 Mintenbeck, A. Alegría, M. Craig, S. Langsdorf, S. Löschke, V. Möller, A. Okem, B.
736 Rama (eds.). Cambridge University Press. Cambridge University Press, Cambridge, UK
737 and New York, NY, USA, 3056 pp., doi:10.1017/9781009325844

- 738 Ji, R., Edwards, M., Mackas, D. L., Runge, J. A., & Thomas, A. C. (2010). Marine plankton
739 phenology and life history in a changing climate: current research and future
740 directions. *Journal of plankton research*, 32(10), 1355-1368.
741 <https://doi.org/10.1093/plankt/fbq062>
- 742 Jönsson, P., & Eklundh, L. (2004). TIMESAT—a program for analyzing time-series of satellite
743 sensor data. *Computers & geosciences*, 30(8), 833-845.
744 <https://doi.org/10.1016/j.cageo.2004.05.006>
- 745 Kohonen, T. (1982). Self-organized formation of topologically correct feature maps. *Biological*
746 *cybernetics*, 43(1), 59-69. <https://doi.org/10.1007/BF00337288>
- 747 Kohonen, T. (1990). The self-organizing map. *Proceedings of the IEEE*, 78(9), 1464-1480.
748 <https://doi.org/10.1109/5.58325>
- 749 Lellouche, J. M., Greiner, E., Le Galloudec, O., Garric, G., Regnier, C., Drevillon, M., ... & Le
750 Traon, P. Y. (2018). Recent updates to the Copernicus Marine Service global ocean
751 monitoring and forecasting real-time 1/12° high-resolution system. *Ocean Science*, 14(5),
752 1093-1126. 10.5194/os-14-1093-2018
- 753 Leyba, I. M., Solman, S. A., & Saraceno, M. (2019). Trends in sea surface temperature and air–
754 sea heat fluxes over the South Atlantic Ocean. *Climate Dynamics*, 53, 4141-4153.
755 <https://doi.org/10.1007/s00382-019-04777-2>
- 756 Liu, Y., Weisberg, R. H., & Mooers, C. N. (2006). Performance evaluation of the self-organizing
757 map for feature extraction. *Journal of Geophysical Research: Oceans*, 111(C5).
758 <https://doi.org/10.1029/2005JC003117>
- 759 Liu, Y., Weisberg, R. H., Vignudelli, S., & Mitchum, G. T. (2016). Patterns of the loop current
760 system and regions of sea surface height variability in the eastern Gulf of Mexico

- 761 revealed by the self-organizing maps. *Journal of Geophysical Research: Oceans*, 121(4),
762 2347-2366. <https://doi.org/10.1002/2015JC011493>
- 763 Longhurst, A. R. (2010). *Ecological geography of the sea*. Elsevier.
- 764 Lucas, A. J., Guerrero, R. A., Mianzan, H. W., Acha, E. M., & Lasta, C. A. (2005). Coastal
765 oceanographic regimes of the northern Argentine continental shelf (34–43 S). *Estuarine,
766 Coastal and Shelf Science*, 65(3), 405-420.
- 767 Lusquiños, A. (1971). *Aportes al conocimiento de las masas de agua del Atlántico
768 Sudoccidental* (Vol. 659). Servicio de Hidrografía Naval.
- 769 Lutz, V. A., Segura, V., Dogliotti, A. I., Gagliardini, D. A., Bianchi, A. A., & Balestrini, C. F.
770 (2010). Primary production in the Argentine Sea during spring estimated by field and
771 satellite models. *Journal of Plankton Research*, 32(2), 181-195.
772 <https://doi.org/10.1093/plankt/fbp117>
- 773 Maritorena, S., d'Andon, O. H. F., Mangin, A., & Siegel, D. A. (2010). Merged satellite ocean
774 color data products using a bio-optical model: Characteristics, benefits and
775 issues. *Remote Sensing of Environment*, 114(8), 1791-1804.
776 <https://doi.org/10.1016/j.rse.2010.04.002>
- 777 Marrari, M., Piola, A. R., & Valla, D. (2017). Variability and 20-year trends in satellite-derived
778 surface chlorophyll concentrations in large marine ecosystems around south and western
779 Central America. *Frontiers in Marine Science*, 4, 372.
780 <https://doi.org/10.3389/fmars.2017.00372>
- 781 Marrari, M., Signorini, S. R., McClain, C. R., Pájaro, M., Martos, P., Viñas, M. D., ... & Buratti,
782 C. (2013). Reproductive success of the Argentine anchovy, *Engraulis anchoita*, in

- 783 relation to environmental variability at a mid-shelf front (Southwestern Atlantic Ocean). *Fisheries Oceanography*, 22(3), 247-261. , <https://doi.org/10.1111/fog.12019>
- 784
- 785 Martos, P., & Piccolo, M. C. (1988). Hydrography of the Argentine continental shelf between 38
- 786 and 42 S. *Continental Shelf Research*, 8(9), 1043-1056.
- 787 Matano, R. P., & Palma, E. D. (2008). On the upwelling of downwelling currents. *Journal of*
- 788 *Physical Oceanography*, 38(11), 2482-2500.
- 789 Matano, R. P., Palma, E. D., & Combes, V. (2019). The Burdwood bank circulation. *Journal of*
- 790 *Geophysical Research: Oceans*, 124(10), 6904-6926.
- 791 <https://doi.org/10.1029/2019JC015001>
- 792 Palmer, S. C., Odermatt, D., Hunter, P. D., Brockmann, C., Presing, M., Balzter, H., & Tóth, V.
- 793 R. (2015). Satellite remote sensing of phytoplankton phenology in Lake Balaton using 10
- 794 years of MERIS observations. *Remote Sensing of Environment*, 158, 441-452.
- 795 <https://doi.org/10.1016/j.rse.2014.11.021>
- 796 Pasquini, A. I., & Depetris, P. J. (2010). ENSO-triggered exceptional flooding in the Paraná
- 797 River: where is the excess water coming from?. *Journal of hydrology*, 383(3-4), 186-193.
- 798 <https://doi.org/10.1016/j.jhydrol.2009.12.035>
- 799 Racault, M. F., Le Quéré, C., Buitenhuis, E., Sathyendranath, S., & Platt, T. (2012).
- 800 Phytoplankton phenology in the global ocean. *Ecological Indicators*, 14(1), 152-163.
- 801 <https://doi.org/10.1016/j.ecolind.2011.07.010>
- 802 Risaro, D. B., Chidichimo, M. P., & Piola, A. R. (2022). Interannual variability and trends of sea
- 803 surface temperature around Southern South America. *Frontiers in Marine Science*, 9,
- 804 213. <https://doi.org/10.3389/fmars.2022.829144>

- 805 Rivas, A. L., & Beier, E. J. (1990). Temperature and salinity fields in the north patagonian
806 gulfs. *Oceanológica acta*, 13(1), 15-20.
- 807 Rivas, A. L., & Pisoni, J. P. (2010). Identification, characteristics and seasonal evolution of
808 surface thermal fronts in the Argentinean Continental Shelf. *Journal of Marine*
809 *Systems*, 79(1-2), 134-143. <https://doi.org/10.1016/j.jmarsys.2009.07.008>
- 810 Romero, S. I., Piola, A. R., Charo, M., & Garcia, C. A. E. (2006). Chlorophyll-a variability off
811 Patagonia based on SeaWiFS data. *Journal of Geophysical Research: Oceans*, 111(C5).
812 <https://doi.org/10.1029/2005JC003244>
- 813 Salgado-Hernanz, P. M., Racault, M. F., Font-Muñoz, J. S., & Basterretxea, G. (2019). Trends in
814 phytoplankton phenology in the Mediterranean Sea based on ocean-colour remote
815 sensing. *Remote Sensing of Environment*, 221, 50-64.
816 <https://doi.org/10.1016/j.rse.2018.10.036>
- 817 Sathyendranath, S., Brewin, R. J., Brockmann, C., Brotas, V., Calton, B., Chuprin, A., ... & Platt,
818 T. (2019). An ocean-colour time series for use in climate studies: the experience of the
819 ocean-colour climate change initiative (OC-CCI). *Sensors*, 19(19), 4285.
820 doi:10.3390/s19194285
- 821 Saraceno, M., Provost, C., & Lebbah, M. (2006). Biophysical regions identification using an
822 artificial neuronal network: A case study in the South Western Atlantic. *Advances in*
823 *Space Research*, 37(4), 793-805. <https://doi.org/10.1016/j.asr.2005.11.005>
- 824 Saraceno, M., Provost, C., & Piola, A. R. (2005). On the relationship between satellite-retrieved
825 surface temperature fronts and chlorophyll a in the western South Atlantic. *Journal of*
826 *Geophysical Research: Oceans*, 110(C11). <https://doi.org/10.1029/2004JC002736>

- 827 Sallée, J. B., Speer, K. G., & Rintoul, S. R. (2010). Zonally asymmetric response of the Southern
828 Ocean mixed-layer depth to the Southern Annular Mode. *Nature Geoscience*, 3(4), 273-
829 279. <https://doi.org/10.1038/ngeo812>
- 830 Segura, V., Silva, R. I., Clara, M. L., Martos, P., Cozzolino, E., & Lutz, V. A. (2021). Primary
831 production and plankton assemblages in the fisheries ground around San Jorge Gulf
832 (Patagonia) during spring and summer. *Plankton and Benthos Research*, 16(1), 24-39.
833 <https://doi.org/10.3800/pbr.16.24>
- 834 Shi, K., Zhang, Y., Zhang, Y., Li, N., Qin, B., Zhu, G., & Zhou, Y. (2019). Phenology of
835 phytoplankton blooms in a trophic lake observed from long-term MODIS
836 data. *Environmental science & technology*, 53(5), 2324-2331.
837 <https://doi.org/10.1021/acs.est.8b06887>
- 838 Shiskin, J. (1978). Seasonal adjustment of sensitive indicators. In *Seasonal Analysis of Economic*
839 *Time Series* (pp. 97-104). NBER.
- 840 Sigman, D. M., Hain, M. P., & Haug, G. H. (2010). The polar ocean and glacial cycles in
841 atmospheric CO₂ concentration. *Nature*, 466(7302), 47-55.
842 <https://doi.org/10.1038/nature09149>
- 843 Signorini, S. R., Garcia, V. M., Piola, A. R., Evangelista, H., McClain, C. R., Garcia, C. A., &
844 Mata, M. M. (2009). *Further studies on the physical and biogeochemical causes for large*
845 *interannual changes in the Patagonian Shelf spring-summer phytoplankton bloom*
846 *biomass* (No. 200900836).
- 847 Signorini, S. R., Garcia, V. M., Piola, A. R., Garcia, C. A., Mata, M. M., & McClain, C. R.
848 (2006). Seasonal and interannual variability of calcite in the vicinity of the Patagonian
849 shelf break (38 S–52 S). *Geophysical research letters*, 33(16).

- 850 Spalding, M. D., Fox, H. E., Allen, G. R., Davidson, N., Ferdaña, Z. A., Finlayson, M. A. X., ...
851 & Robertson, J. (2007). Marine ecoregions of the world: a bioregionalization of coastal
852 and shelf areas. *BioScience*, 57(7), 573-583. <https://doi.org/10.1641/B570707>
- 853 Valla, D., & Piola, A. R. (2015). Evidence of upwelling events at the northern Patagonian shelf
854 break. *Journal of Geophysical Research: Oceans*, 120(11), 7635-7656.
855 <https://doi.org/10.1002/2015JC011002>
- 856 Vantrepotte, V., & Mélin, F. (2009). Temporal variability of 10-year global SeaWiFS time-series
857 of phytoplankton chlorophyll a concentration. *ICES Journal of Marine Science*, 66(7),
858 1547-1556. <https://doi.org/10.1093/icesjms/fsp107>
- 859 Vantrepotte, V., & Mélin, F. (2011). Inter-annual variations in the SeaWiFS global chlorophyll a
860 concentration (1997–2007). *Deep Sea Research Part I: Oceanographic Research*
861 *Papers*, 58(4), 429-441. <https://doi.org/10.1016/j.dsr.2011.02.003>
- 862 Vesanto, J., & Alhoniemi, E. (2000). Clustering of the self-organizing map. *IEEE Transactions*
863 *on neural networks*, 11(3), 586-600. <https://doi.org/10.1109/72.846731>
- 864 Vesanto, J., Himberg, J., Alhoniemi, E., Parhankangas, J., Team, S. O. M. T., & Oy, L.
865 (2000). *SOM toolbox for Matlab 5* (Vol. 57, No. 2). Technical report.
- 866 Williams, G. N., Pisoni, J. P., Solís, M. E., Romero, M. A., Ocampo-Reinaldo, M., Svendsen, G.
867 M., ... & González, R. A. C. (2021). Variability of phytoplankton biomass and
868 environmental drivers in a semi-enclosed coastal ecosystem (San Matías Gulf,
869 Patagonian Continental Shelf, Argentina) using ocean color remote sensing (MODIS) and
870 oceanographic field data: Implications for fishery resources. *Journal of Marine*
871 *Systems*, 224, 103615. <https://doi.org/10.1016/j.jmarsys.2021.103615>

- 872 Williams, G. N., Dogliotti, A. I., Zaidman, P., Solis, M., Narvarte, M. A., Gonzalez, R. C., ... &
873 Gagliardini, D. A. (2013). Assessment of remotely-sensed sea-surface temperature and
874 chlorophyll-a concentration in San Matías Gulf (Patagonia, Argentina). *Continental Shelf
875 Research*, 52, 159-171. <https://doi.org/10.1016/j.csr.2012.08.014>
- 876 Williams, G. N., & Nocera, A. C. (2023). Bio-optical trends of waters around Valdés Biosphere
877 Reserve: An assessment of the temporal variability based on 20 years of ocean color
878 satellite data. *Marine Environmental Research*, 105923.
879 <https://doi.org/10.1016/j.marenvres.2023.105923>
- 880 Yala, K., Niang, N. D., Brajard, J., Mejia, C., Ouattara, M., El Hourany, R., ... & Thiria, S.
881 (2020). Estimation of phytoplankton pigments from ocean-color satellite observations in
882 the Senegalo–Mauritanian region by using an advanced neural classifier. *Ocean
883 Science*, 16(2), 513-533. <https://doi.org/10.5194/os-16-513-2020>
- 884 Yu, S., Bai, Y., He, X., Li, T., & Gong, F. (2023). A new merged dataset of global ocean
885 chlorophyll-a concentration for better trend detection. *Frontiers in Marine Science*, 10,
886 48. <https://doi.org/10.3389/fmars.2023.1051619>
- 887 Zhai, L., Platt, T., Tang, C., Sathyendranath, S., & Walne, A. (2013). The response of
888 phytoplankton to climate variability associated with the North Atlantic Oscillation. *Deep
889 Sea Research Part II: Topical Studies in Oceanography*, 93, 159-168.
890 <https://doi.org/10.1016/j.dsr2.2013.04.009>
- 891 Zoljoodi, M., Moradi, M., & Moradi, N. (2022). Seasonal and interannual cycles of total
892 phytoplankton phenology metrics in the Persian Gulf using ocean color remote
893 sensing. *Continental Shelf Research*, 237, 104685.
894 <https://doi.org/10.1016/j.csr.2022.104685>